JOURNAL OF APPLIED ELECTROCHEMISTRY **10** (1980) 765–774

# *Effect of nickel impurities on zinc electrodeposition*

R. FRATESI, G. ROVENTI

*Istituto di Chimica, Università di Ancona, Ancona, Italy*

M. MAJA, N. PENAZZI

*Istituto di Elettrochimica e Chimica Fisica, Politecnico di Torino, Torino, Italy*

Received 9 January 1980

The kinetics of nickel–zinc co-deposition and the effect of nickel on zinc morphology have been studied by means of chemical analysis, X-ray diffraction and SEM observations of cathodic deposits obtained in various experimental conditions, including acid and alkaline baths. It has been shown that nickel ions, even if present in the electrolyte at very low concentrations (1 ppm), do not deposit under mass transport controlled conditions but are dragged by zinc ions whose concentration influences the nickel current. With regard to zinc morphology, it has been observed that nickel reduces the grain size of the zinc crystals formed during the electrodeposition.

## 1. Introduction

The effect of impurities on zinc electrodeposition has been the subject of several earlier investigations [1–25] carried out particularly for acid zinc sulphate baths in order to determine the best working conditions for industrial cells and to control the purity of the electrolytes. More recently, the effect of metallic impurities on zinc electrocrystallization has been considered [26].

Maja *et al.* [24, 25] showed that the addition of some impurities to acid sulphate baths drastically lowers the zinc current efficiency only after a certain time. At the beginning of the electrolysis, the zinc current efficiency reaches and maintains a relatively high value (greater than 90%). After a period, strongly dependent on temperature and sulphuric acid concentration, the current efficiency rapidly decreases and the zinc deposit dissolves in the electrolyte. After complete dissolution, a new zinc deposition takes place. These deposition–dissolution cycles repeat regularly with time and are related to periodic variations of cathodic potential under galvanostatic conditions and to periodic current variations under potentiostatic conditions. The period of the cycles is not constant but increases with time until zinc deposition does not occur any more.

From measurements of induction time the impurities have been classified in order of their noxious effect on the electrodeposition. The effect decreases in the order

Ge Sb Ni Co Bi Cu As Sn Fe.

This classification, with the exception of Ge and Fe, can be correlated with the hydrogen overvoltage scale.

In this paper we have taken into account those aspects of the problem that have not yet been thoroughly examined, such as the discharge mechanism of impurities and their influence on zinc deposit morphology, using the example of zinc–nickel co-deposition. The present study has been extended to alkaline baths for the evident implications for Ni–Zn batteries.

Zinc–nickel co-deposition has been studied tracing the cathodic polarization curves for hydrogen, zinc and nickel discharge in various experimental conditions. The influence of nickel on the deposit morphology has been studied by means of SEM and X-ray diffraction techniques.

## 2. Experimental

The electrolysis cell consisted of a glass vessel maintained at constant temperature (± 0.2° C); the cathode was a pure metal cylinder, Al for acid and Zn for alkaline baths, with a diameter of 1.5 cm,

0021–891X/80/060765–10$03.00/0  

embedded in acrylic resin. The counter electrode was a pure Pt sheet. The reference electrode was of mercurous sulphate for acid baths and mercurous oxide for alkaline electrolytes. Before each test the surface of the working electrode was activated with emery paper.

All solutions were prepared using analytical grade chemicals and bidistilled water. Nickel impurity was added to acid sulphate baths as nickel sulphate. In alkaline baths, nickel impurity was introduced by adding freshly prepared $Ni(OH)_2$ in the quantity needed to saturate the zincate solution. The suspension of nickel hydroxide in zincate was stirred for 20 hours at the same temperature as the electrochemical tests and then filtered. The electrolyte was not stirred during electrolysis.

The partial currents for hydrogen, nickel and zinc were determined by measuring the hydrogen volume evolved per unit of time, the weight of the deposit and its composition. The data concerning hydrogen were obtained by measuring, in steady gas flow conditions, the time needed to collect a variable volume of hydrogen (from 0.2 to 0.5 $cm^3$) at the cathode. The results reported in this paper refer to tests in which the hydrogen partial current so calculated remained constant for at least 30 min under stationary electrochemical conditions.

Measurements regarding zinc and nickel were made after different times of electrolysis (30, 60, 90 and 120 min). The results reported below are mean values of discharge rate calculated from data corresponding to various times of electrolysis. At the end of every test the cathode was taken away from the cell with the electric circuit still closed to avoid zinc dissolution and rinsed in pure water. The deposit was then removed, washed in bidistilled water and ethyl alcohol and dried in air at 60° C. The deposit was weighed and dissolved in $HNO_3$ 1:1 solution which was analysed to determine the amount of nickel co-deposited with zinc. In other cases zinc deposits were observed at the scanning electron microscope (Siemens Omniscan model) and analysed by X-ray diffraction (Philips diffractometer). The amount of nickel in zinc deposits was determined using the atomic absorption technique (Perkin Elmer Atomic Absorption Spectrophotometer, model 300).

According to the procedure used for hydrogen volume measurement, we took into account only those tests in which the weight of zinc increased proportionally with time. In every case the charge for hydrogen evolution and zinc deposition was the same as the charge used in the electrolysis. Thus, in spite of the fact that the data reported are mean values, the results are consistent and can be referred to stationary conditions.

The amount of nickel contaminating the surface of the cathode during electrolysis in the acid bath was determined by atomic absorption analysis taking the cathode away from the solution just at the end of a deposition–dissolution cycle and dissolving the nickel present on the aluminium surface in $HNO_3$ 1:1 solution. The results were always compared with the data obtained from analysis of an uncontaminated aluminium cathode.

During the tests, carried out under galvanostatic conditions, the cathode potential was recorded as a function of time. From the amount of nickel, zinc and hydrogen discharged and from the cathode potential values the partial polarization curves for these elements were traced. All the tests were repeated three times with excellent agreement of the data.

## 3. Results and discussion

### 3.1. *Electrodeposition from sulphate baths*

As the length of the deposition–dissolution cycles varies with continuity from a few seconds to several hours according to temperature, sulphuric acid concentration, current density and amount of nickel contained in the electrolyte, it seemed convenient to divide the experimental results into two groups. The first group concerns depositions from solutions having a sulphuric acid concentration greater than 3 N, for which examination of the deposit is impossible due to the short length of the induction time. The second group refers to depositions from baths with a sulphuric acid concentration lower than 3 N. In this case the deposit is stable enough to be analysed.

*3.1.1. Sulphate baths with $H_2SO_4$ concentration greater than 3 N.* Zinc electrodeposition under galvanostatic conditions from these baths is characterized by variations of the current efficiency and electrode potential corresponding to periodical

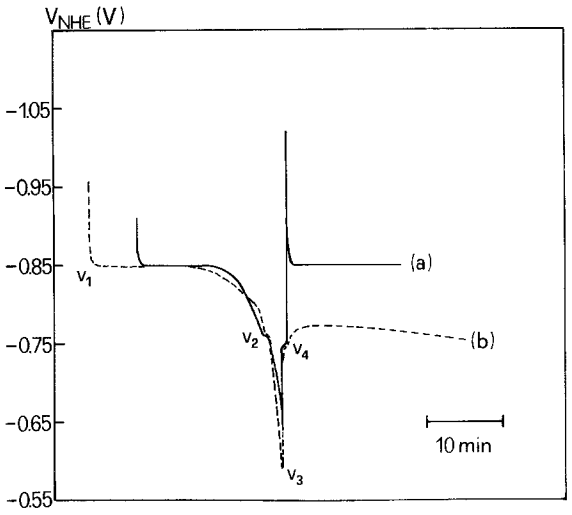


Fig. 1. Cathodic potential versus time curve for (a) the initial and (b) the final deposition–dissolution cycles. Electrolysis conditions: 50 mA $cm^{-2}$ current density; 4 N $H_2SO_4$; 50 g $l^{-1}$ $Zn^{2+}$; 50 mg $l^{-1}$ $Ni^{2+}$; 50° C.

depositions and redissolutions of the metal. As has been mentioned above, this cycle continues for a long time until zinc cannot deposit any longer.

The cathodic processes can be studied by recording potential versus time curves, two of which are reported in Fig. 1. The first of these curves refers to the initial conditions of electrolysis; the second one is the last curve obtained. In order to get a better understanding of the phenomena occurring at the various stages of the process, additional tests were devised. These tests led to the determination of:

(a) The zinc corrosion potential in the solutions used to deposit the metal.

(b) The hydrogen evolution overvoltage on pure nickel, aluminum and zinc electrodes and on aluminium electrodes contaminated by nickel in zinc-free electrolyte having the same acidity as the ones used for zinc electrodeposition.

(c) The potential versus time curves for the hydrogen evolved during the formation of the first zinc monolayer on aluminium.

From the information obtained, the cathode potential values (denoted in Fig. 1 as $V_1$–$V_4$), can be defined as follows: $V_1$ corresponds to the zinc electrodeposition potential, $V_2$ is the zinc corrosion potential, $V_3$ is related to hydrogen evolution on the aluminium cathode contaminated by nickel, and $V_4$ refers to hydrogen evolution on aluminium during the deposition of the first zinc monolayer.

As can be seen in Fig. 1, $V_1$, $V_2$ and $V_4$ maintain a constant value during electrolysis while $V_3$ is slightly decreased. The $V_3$–$V_4$ step becomes more persistent with time until, after the last dissolution, the electrode potential assumes a value between $V_3$ and $V_4$, lower than the $Zn$–$Zn^{2+}$ couple potential. This fact suggests a correlation between the frequency of the cycles and the time needed for the formation of the first zinc monolayer, which seems to increase with the cathode contamination.

We have also carried out tests to determine the electrochemical conditions of zinc electrodeposition on nickel and the amount of nickel contaminating the aluminium surface. With regard to zinc deposition on nickel we have found a threshold value of current density beyond which zinc does not deposit regardless of the duration of the cathodic polarisation. Fig. 2, traced for a cathode polarisation time of 15 min, shows that this threshold value is related to sulphuric acid concentration. Cathode contamination has been studied by interrupting electrolysis at the end of one of the cyclic dissolutions and analysing the cathode surface. Analyses of cathodes removed from the cell at different times of electrolysis revealed that the amount of nickel contaminating the electrode surface grows with the number of cycles (Fig. 3).

From the results obtained we derived the following explanation of the deposition–dissolution phenomenon. Let us first consider zinc electrodeposition from nickel-free acid sulphate baths: in this case the first monolayer of deposit forms very slowly owing to the great difference of hydrogen overvoltage values on zinc and aluminium.

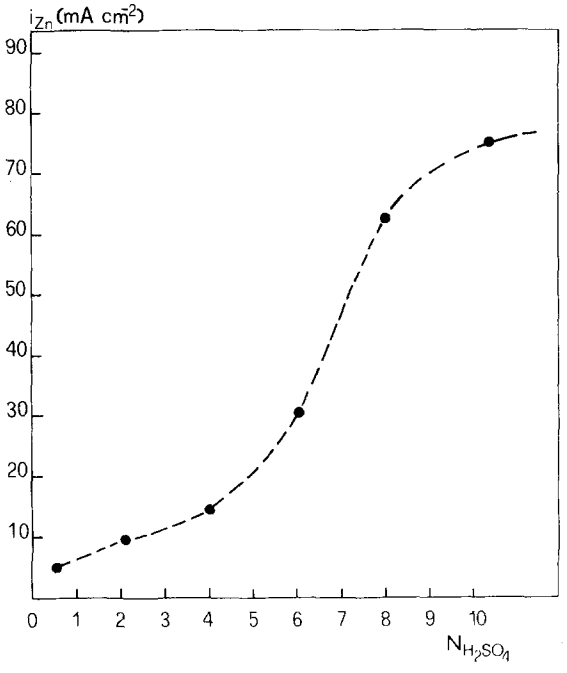


Fig. 2. Minimum current density at which zinc deposits within 15 min on a nickel cathode, for various values of $H_2SO_4$ concentration in the electrolyte. Electrolysis conditions: 50 g l$^{-1}$ $Zn^{2+}$; 25° C.

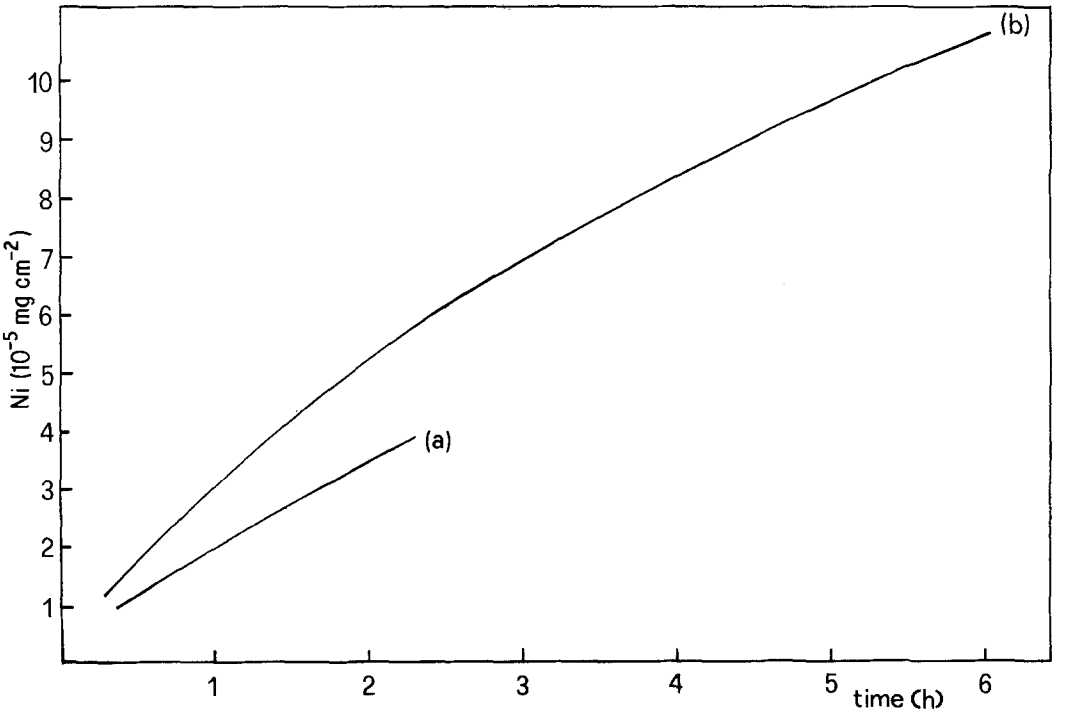


Fig. 3. Amount of nickel per unit area of cathode surface found on the electrodic surface after several depositions and redissolutions of zinc deposits. Various tests were carried out at different values of current density ranging between (a) 25 mA cm$^{-2}$ and (b) 100 mA cm$^{-2}$. Electrolysis conditions: 4 N $H_2SO_4$; 50 g l$^{-1}$ $Zn^{2+}$; 50 mg l$^{-1}$ $Ni^{2+}$; 50° C.

At the beginning of the electrolysis the cathode potential is lower than the $Zn–Zn^{2+}$ couple. Therefore zinc discharges on aluminium in the so-called underpotential condition, hydrogen evolution being the preferred electrochemical process. Later on zinc depositing on the cathode increases the hydrogen overvoltage and the cathode potential is shifted towards negative values until massive zinc deposition occurs with a decrease of hydrogen evolution.

When the electrolyte contains nickel as an impurity, local deposition of nickel occurs together with the formation of the first monolayer of zinc. The cathode areas covered by nickel constitute centres for hydrogen evolution and a longer time is required for the formation of the first zinc monolayer. As zinc deposition goes on, nickel co-deposits, forming new centres of hydrogen evolution. This causes a decrease of hydrogen overvoltage and zinc partial current until the electrode potential reaches the zinc corrosion potential $V_2$ (Fig. 1). In these conditions the electrolysis current is the difference between the currents for hydrogen evolution and zinc dissolution and is much lower (from 5 to 8 times) than the partial currents. The electrode potential has, at first, a value near the zinc reversible potential due to the overpotential value for zinc dissolution which is low even at very high currents. As zinc dissolution does not occur layer by layer but spreads from certain spots on the electrodic surface, the deposited zinc surface decreases with time with an abrupt variation towards the end of the dissolution. Correspondingly, the zinc dissolution overpotential increases and the electrode potential shifts towards less negative values according to the trend of the polarization curve for hydrogen discharge, abruptly increasing as the last part of zinc dissolves.

When all the zinc deposited has dissolved, together with part of the co-deposited nickel, the aluminum surface, contamined by some nickel, is ready for a new deposition–dissolution cycle. This cycle phenomenon continues until the amount of nickel contamining the cathode, which increases with every dissolution, completely prevents the discharge of zinc ions.

*3.1.2. Sulphate baths with $H_2SO_4$ concentration lower than 3 N.* During electrodeposition from acid sulphate baths under galvanostatic conditions, electrode potential and current efficiency remain constant for several hours if the $H_2SO_4$ concentration is lower than 3 N. It is thus possible to determine zinc, hydrogen and nickel partial currents at various electrode potentials. Figs. 4 and

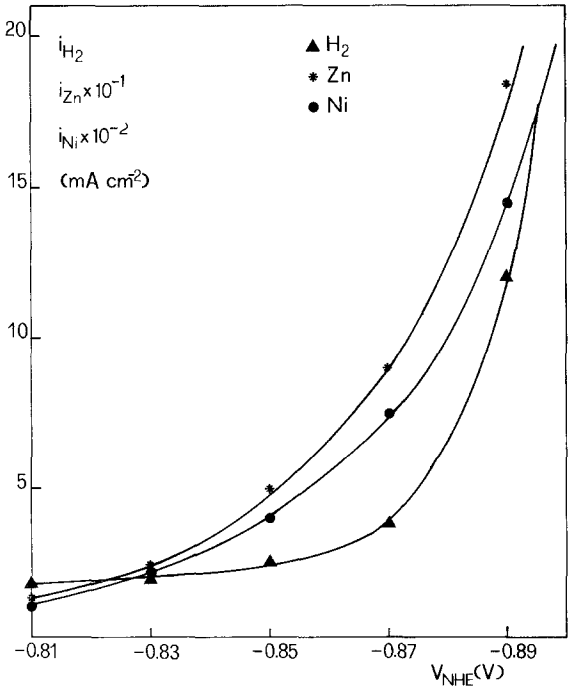


Fig. 4. Polarization curves (current density $i$ versus cathode potential $V$) for zinc and nickel deposition and hydrogen evolution. Electrolysis conditions: 0.5 N $H_2SO_4$; 50 g $l^{-1}$ $Zn^{2+}$; 50 ppm $Ni^{2+}$; 38° C.

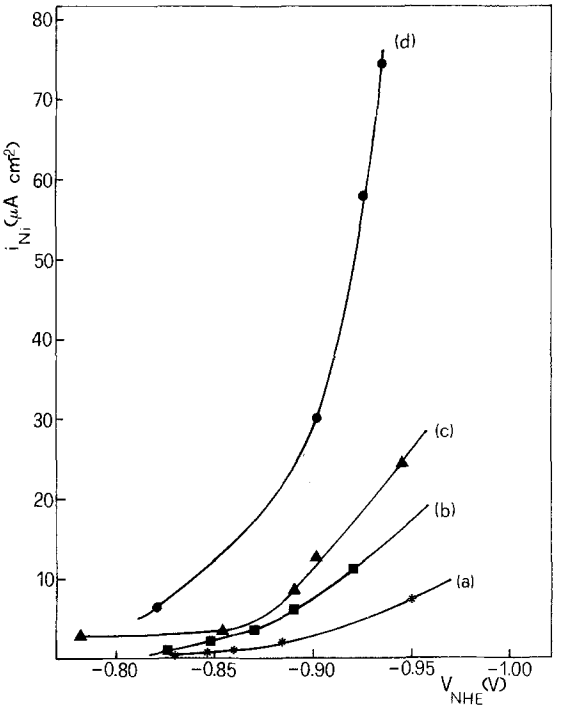


Fig. 5. Polarization curves for nickel deposition from electrolytes containing the following amounts of nickel ions: (a) 1 ppm, (b) 5 ppm, (c) 10 ppm, (d) 50 ppm. Electrolysis conditions: 0.5 N $H_2SO_4$; 50 g l$^{-1}$ $Zn^{2+}$; 25° C.

5 report two groups of polarization curves referring to zinc, hydrogen and nickel (Fig. 4) and to various concentrations of nickel ions (Fig. 5).

Investigations on the parameters influencing nickel discharge rate showed a dependence on electrode potential, zinc and sulphate concentrations and temperature:

$$i_{Ni} = i([Ni^{2+}], [Zn^{2+}], [SO_4^{2-}], V, T)$$

as shown in Figs. 6–8. From Fig. 5 it can be deduced that nickel ions, even if present in very low concentration, do not deposit in limiting current conditions*. The discharge of nickel ions in the zinc lattice is thus a highly irreversible process. This can perhaps be related to the fact that nickel is very scarcely soluble in zinc [27] and that nickel atoms need a high energy to crystallize with zinc.

The linear relation between nickel partial current density and zinc concentration, verified for various temperatures from 10–40° C, (Fig. 8) is particularly important because it shows one of the possible mechanisms for nickel ion discharge. Such ions seem to be transferred from the solution to the electrode by zinc ions. The phenomenon could take place via formation of a co-ordination complex between nickel, zinc and sulphate ions: some studies seem to confirm the existence of such complexes [28].

The morphology of zinc deposits from pure sulphate baths has already been extensively studied by several authors [26, 29, 30]. For a wide range of current density values (10–200 mA cm$^{-2}$) the deposit surface consists of casually oriented blocks of parallel platelets packed together, as can be seen from the micrograph in Fig. 9. X-ray analysis of the deposit shows a preferential orientation of the grains, corresponding to the (101) plane of lower rate of growth. The grain size increases as current density increases (Fig. 10). Temperature exerts a strong influence on the morphology and the orientation of the deposits: Fig. 11 shows the appearance at 38° C of hexagonal platelets, mainly parallel to the substrate.

The presence of nickel in the electrodeposition baths influences the deposit morphology causing a reduction of grain size as shown in Fig. 12. Such a reduction is of course more evident as the amount of nickel increases. Correspondingly, X-ray spectra show a marked increase in intensity of the lines corresponding to (002), (100), (102) and (110) planes (Table 1). It seems likely that the introduction of nickel atoms in the zinc lattice reduces the rate of growth for these planes and, consequently, the nucleation rate increases.

SEM analysis revealed the existence of deep circular holes on the surface of the deposits obtained from Ni-containing baths (Fig. 13), which, from the beginning of electrolysis, form on those parts of the cathodic surface contaminated by nickel and are centres of hydrogen evolution.

*Table 1. Influence of nickel on the crystallographic orientation of zinc deposits. Electrolysis conditions: 0.5 N $H_2SO_4$; 50 g l$^{-1}$ $Zn^{2+}$; 10 mA cm$^{-2}$ current density; 25° C*

| | *Orientation* | | | | | |
|---|---|---|---|---|---|---|
| $Ni^{2+}$(ppm) | (002) | (100) | (101) | (102) | (103) | (110) |
| 0 | 4.3 | 20.2 | 100 | 16 | 10.6 | 9.9 |
| 50 | 10.6 | 12 | 100 | 18.3 | 13.4 | 5.7 |
| 150 | 37.5 | 23.7 | 100 | 38.6 | 28 | 15 |

* Assuming a value of $10^{-5}$ cm$^2$ s$^{-1}$ for the diffusion coefficient and a value of $2.0 \times 10^{-2}$ cm for the diffusion layer thickness, a limiting diffusion current density of about 100 μA cm$^{-2}$ mM$^{-1}$ has been estimated.

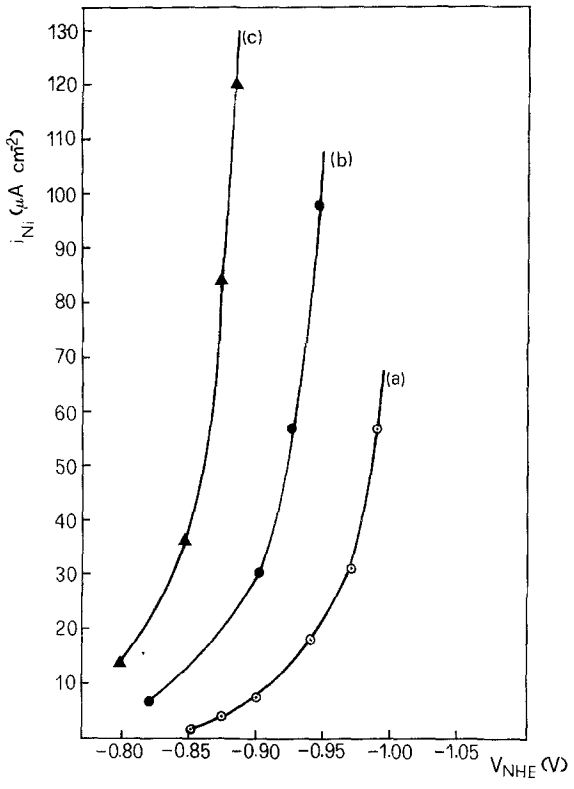


Fig. 6. Polarization curves for nickel deposition at (a) 10° C, (b) 25° C, (c) 38° C. Electrolysis conditions: 0.5 N $H_2SO_4$; 50 g l$^{-1}$ $Zn^{2+}$; 50 ppm $Ni^{2+}$.

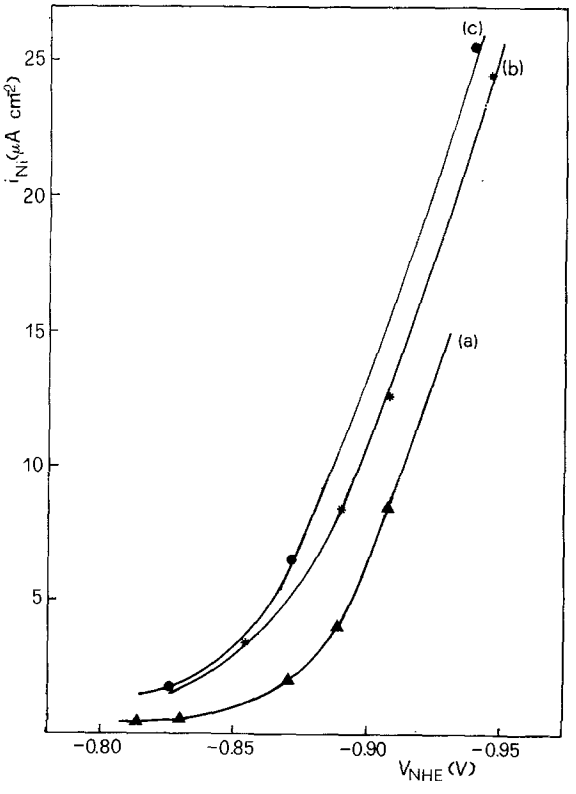


Fig. 7. Polarization curves for nickel deposition from electrolytes containing: (a) 2.2 M $Cl^-$, (b) 1 M $SO_4^{2-}$, (c) 1.2 M $SO_4^{2-}$. Electrolysis conditions: 50 g l$^{-1}$ $Zn^{2+}$; 10 ppm $Ni^{2+}$; 25° C.

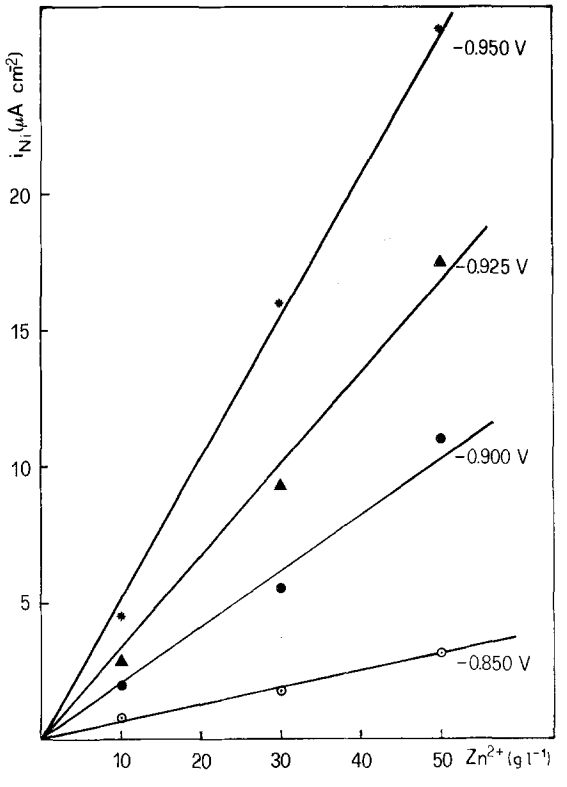


Fig. 8. Dependence of nickel partial current density on $Zn^{2+}$ concentration for tests carried out at different cathodic potentials. Electrolysis conditions: 0.5 N $H_2SO_4$; 10 ppm $Ni^{2+}$; 25° C.

These holes are generally very narrow and exhibit a potential difference, decreasing from the top to the bottom, between zinc constituting the internal surface and the electrolyte according to the electrical resistivity of the solution. So the local electrolysis conditions inside the holes are quite different from the ones on the external electrode surface and the impurities have a greater influence [25]. Due to the lower current density, which is related to zinc electrodeposition on nickel as illustrated in Fig. 2, and to the local depletion of zinc ions, nickel centres are likely to form on the internal surface of the holes. As zinc dissolves, nickel contained inside the deposit appears at the surface

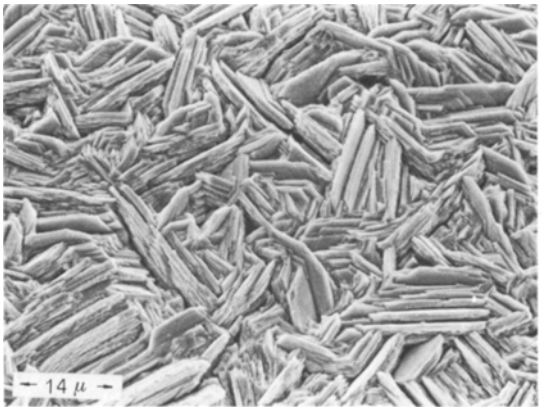


Fig. 9. Zinc deposited at 10 mA cm$^{-2}$ current density from Ni-free electrolyte having the following composition: 0.5 N $H_2SO_4$; 50 g l$^{-1}$ $Zn^{2+}$; 25° C.

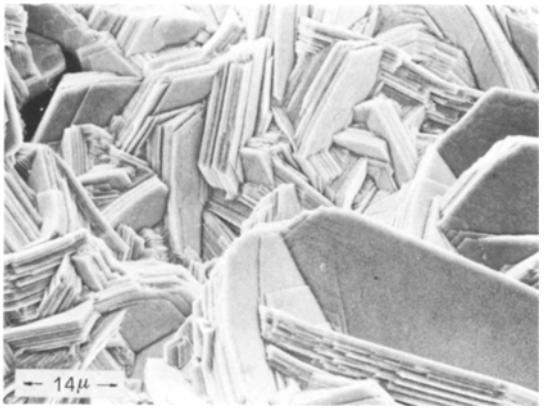


Fig. 10. Zinc deposited at 200 mA cm$^{-2}$ current density from Ni-free electrolyte. Electrolysis conditions: 0.5 N $H_2SO_4$; 50 g l$^{-1}$ $Zn^{2+}$; 25° C.

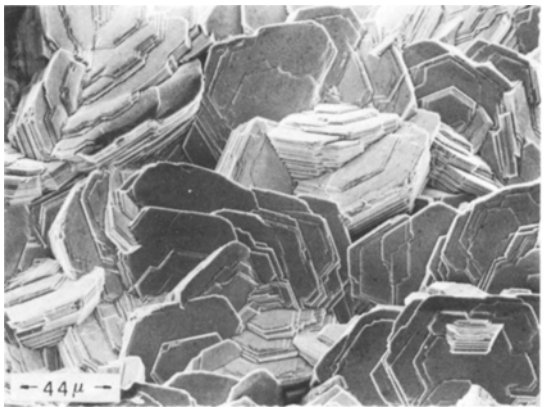


Fig. 11. Zinc deposited at 40° C and 200 mA $cm^{-2}$ from Ni-free electrolyte. Electrolysis conditions: 0.5 N $H_2SO_4$; 50 g $l^{-1}$ $Zn^{2+}$.

and the hydrogen overvoltage locally decreases. This process extends with time to the areas surrounding the holes until the total zinc current efficiency begins to decrease. From this moment on, the corrosion of the contaminated zinc becomes an autocatalytic process and the current efficiency rapidly decreases to zero.

### 3.2. *Electrodeposition from alkaline baths*

The effect of nickel impurity on zinc electrodeposition from zincate solution has been investigated using the same techniques as for acid sulphate baths. The very low solubility of nickel in alkaline baths (approximately 0.6 ppm at 25° C) has made it impossible to vary the amount of nickel added to the electrolyte used in the tests.

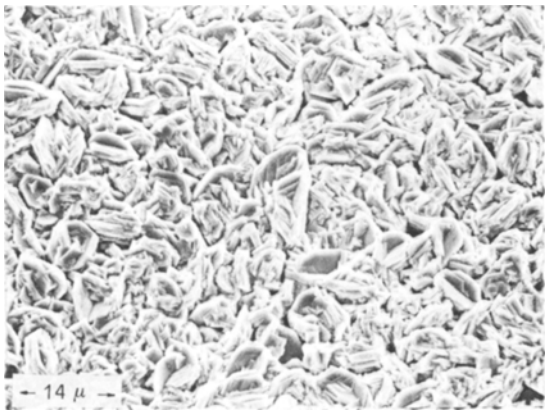


Fig. 12. Zinc electrodeposited from an electrolyte containing 50 ppm of nickel ions at 10 mA $cm^{-2}$ current density. Electrolysis conditions: 0.5 N $H_2SO_4$; 50 g $l^{-1}$ $Zn^{2+}$; 25° C.

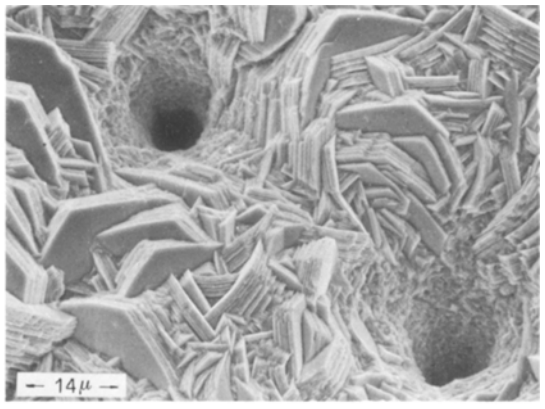


Fig. 13. Zinc electrodeposited from an electrolyte containing 50 ppm of nickel ions at 200 mA $cm^{-2}$ current density. Electrolysis conditions: 0.5 N $H_2SO_4$; 50 g $l^{-1}$ $Zn^{2+}$; 25° C.

Fig. 14 reports the partial polarization curves for zinc, nickel and hydrogen discharge from nickel-saturated solutions of zincate. Tests carried out at various temperatures and with various zincate concentrations show that these parameters do not influence nickel partial current.

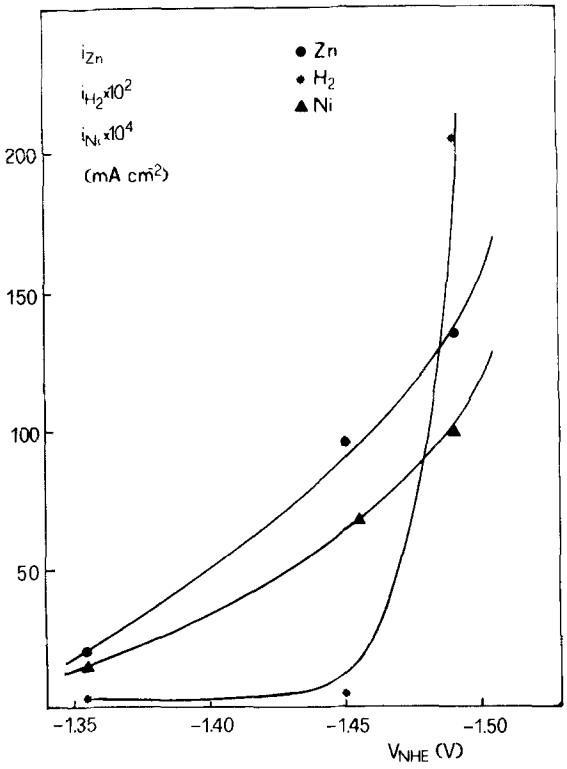


Fig. 14. Polarization curves for zinc and nickel deposition and hydrogen evolution. Electrolysis conditions: 8 N NaOH; 58 g $l^{-1}$ $Zn^{2+}$; 0.6 ppm $Ni^{2+}$; 25° C.

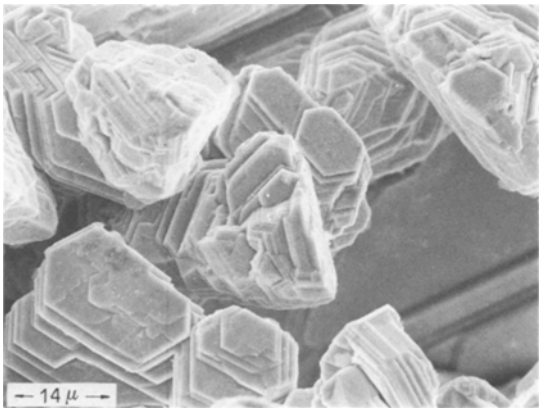


Fig. 15. Zinc deposit obtained from an electrolyte containing 0.6 ppm $Ni^{2+}$ at 25 mA $cm^{-2}$ current density. Electrolysis conditions: 8 N NaOH; 58 $g\,l^{-1}$ $Zn^{2+}$; 25° C.

The low amount of nickel in solution and the low zinc corrosion rates in alkaline baths compared with those in acid ones, hinder the occurrence of dissolution phenomena in the electrolytes. Nevertheless, nickel exerts some influence on zinc deposit morphology. The morphology of zinc deposits from pure alkaline solutions has already been investigated by several authors [31–35] and our results completely confirm their observations.

A disperse, sponge-like deposit is obtained from solutions containing zinc in high concentration (60 $g\,l^{-1}$) and at low current density ($i < 30$ mA $cm^{-2}$). For current densities from 30–100 mA $cm^{-2}$ the deposit consists of hexagonal crystallites. At higher current densities ($i > 100$ mA $cm^{-2}$) dendrites rapidly form. Morphology is also dependent on the amount of zinc ions contained in the electrolyte: a decrease in zinc concentration produces a decrease in the current density threshold for the dendrite formation. X-ray analysis showed that current density and zinc concentration do not change the preferred crystallographic orientations of the deposit which appears to grow in the (101) and (002) planes.

Our tests showed that nickel addition to the zincate solution favours the growth of compact deposits. Hexagonal crystallites can also be seen at low values of current density (Fig. 15). On the contrary, the presence of nickel has no influence on dendrite formation in solutions of both high and low zinc concentration.

## References


[1] L. Cambi, *Elettrotecnica* **9** (1962) 189.
[2] R. Piontelli, *Chim. Ind.* **22** (1940) 109.
[3] G. Scacciati, *Ind. Miner.* **4** (1953) 511.
[4] U. F. Turomshina and V. V. Stender, *J. Appl. Chem., USSR* **28** (1955) 151.
[5] *Idem, ibid* **28** (1955) 347.
[6] *Idem, ibid* **28** (1955) 447.
[7] A. V. Pomosov, E. E. Keymakova and A. I. Levin, *J. Prikl. Khim.* **31** (1958) 734.
[8] G. T. Wever, *J. Metals* **11** (1959) 130.
[9] A. F. Nikiforov and V. V. Stender, *Ukr. Khim. J.* **25** (1959) 18.
[10] G. Z. Kir'yakoy and F. K. Bainietova, *Tr. Inst. Khim. Akad. Nauk Kazakh., USSR* **6** (1960) 86.
[11] M. Kett, *Hutnicke Listy* **16** (1961) 669.
[12] G. C. Bratt, *Electrochem. Technol.* **2** (1964) 323.
[13] G. N. Znamenskii and B. N. Bezyazykov, *J. Prickl. Khim., USSR* **38** (1965) 361.
[14] I. W. Wark, 'Proc. 1st Australian Conf. on Electrochemistry', Pergamon Press, London (1965) p. 889.
[15] J. Kruger and H. Winterhager, *Erzmetall.* **18** (1965) 564.
[16] G. N. Znamenskii and V. M. Serebritskii, *Ukr. Khim. J.* **7** (1965) 703.
[17] G. N. Pakhomova, *Sov. J. Non-Ferrous Metals* **6** (1965) 35.
[18] G. N. Pakhomova and K. L. Ovechnikova, *Zashchitn. Metal Akad. Nauk SSR* **1** (1965) 164.
[19] M. Maja, *Electrochim. Metall.* **4** (1967) 469.
[20] A. D'Este and R. Guerriero, *Montevecchio* **16** (1965) 1.
[21] N. A. Fishman, V. L. Klimenko and K. Y. Nevedrov, *Tsvetn. Metal* **1** (1963) 30.
[22] Yu. N. Tokayev, G. G. Ranney, I. S. Pintchouk, A. A. Saline, P. S. Gouzarov and I. P. Toulenko, 'Teoria i Praktika Metallurgii', 4th edn (1961) p. 184.
[23] F. Laist, F. F. Frick, J. O. Elton and R. B. Caples, *Trans. AIME* **64** (1921) 699.
[24] M. Maja and S. Pozzoli, *Chim. Ind.* **51** (1969) 133.
[25] M. Maja and P. Spinelli, *J. Electrochem. Soc.* **118** (1971) 1538.
[26] D. J. Mackinnon and J. M. Brannen, *J. Appl. Electrochem.* **7** (1977) 451.
[27] F. Paulek, *Z. Metallkd.* **36** (1952) 1.
[28] M. Frias Ferreira Da Rocha and J. Gilbert, *Bull. Soc. Chim. Belg.* **81** (1972) 263.
[29] J. M. Keen and J. P. G. Farr, *J. Electrochem. Soc.* **109** (1962) 8.
[30] R. Sato, *ibid* **106** (1959) 206.
[31] R. D. Naybour, *Electrochim. Acta* **13** (1968) 763.
[32] S. Arouete, K. F. Blurton and H. G. Oswin, *J. Electrochem. Soc.* **116** (1969) 166.
[33] J. O'M. Bockris, Z. Nagy and D. Drazic, *ibid* **120** (1973) 30.
[34] N. Justinijanovic and A. R. Despic, *Electrochim. Acta* **18** (1973) 709.
[35] I. Epelboin, M. Ksouri and R. Wiart, *J. Electroanal. Chem.* **65** (1975) 373.